The International Journal of Advanced Manufacturing Technology (2019) 100:199–208
https://doi.org/10.1007/s00170-018-2570-0

ORIGINAL ARTICLE

Effects of rotation speed of assisted shoulder on microstructure and mechanical properties of 6061-T6 aluminum alloy by dual-rotation friction stir welding

L. Zhou [1,2] · R. X. Zhang [1,2] · X. Y. Hu [1,2] · N. Guo [1,2] · H. H. Zhao [3] · Y. X. Huang [4]

Received: 26 February 2018 / Accepted: 13 August 2018 / Published online: 24 September 2018

Abstract
By adjusting the rotation speed of separated pin and assisted shoulder, dual-rotation friction stir welding can reduce the softened region and improve the properties of joint. In this study, a tool system for dual-rotation friction stir welding was designed. Five-millimeter-thick 6061-T6 aluminum alloy was welded using the self-designed tool system. The effects of rotation speed of assisted shoulder on microstructure and mechanical properties of joints were analyzed. Defect-free joints were obtained under the process parameters used. Fine equiaxed recrystallized grains were found in both weld nugget zone and shoulder affected zone, while the grain size in shoulder affected zone appeared to be much smaller. The microhardness showed a noticeable decline in the weld zone, and the lowest value was located in heat-affected zone. Tensile test results demonstrated that all welded joints fractured at the interface of thermo-mechanically affected zone and heat-affected zone with ductile fracture mode.

Keywords Dual-rotation friction stir welding · Aluminum alloy · Microstructural evolution · Mechanical properties

1 Introduction

Aluminum alloys, as the lightweight structural material, have been widely used in aviation, rail transportation, shipbuilding, and other fields for its benefits of high strength, good fatigue resistance, and excellent corrosion resistance [1, 2]. It is becoming increasingly important to achieve the high-quality joining of aluminum alloy. However, traditional fusion welding of aluminum alloy suffers from problems such as porosity, crack, loss of alloying elements, and the strength of welded joint substantially decreases, which has greatly limited its application [3–7]. Invented by The Welding Institute (TWI) in 1991, friction stir welding (FSW) provides a new approach for the joining of aluminum alloy [8]. FSW solves some common issues in fusion welding of aluminum alloys owing to the nature of solid-state bonding, thus producing the joint with superior properties. After more than 20 years of development, FSW has been successfully applied to nearly all aluminum alloys [9–13].

The heat input during FSW process is relatively lower compared with fusion welding. However, it is still sufficient to cause adverse effects on microstructure while welding heat-treatable aluminum alloys, such as the dissolution and coarsening of strengthening precipitates [12, 14]. Thus, a softened region would form after welding which results in poor joint properties [15, 16]. To reduce the detrimental effects of thermal cycle, dual-rotation FSW (DR-FSW) has been put forward on the basis of conventional FSW [17]. DR-FSW is a newly developed FSW technique which separates the pin and assisted shoulder. It is noteworthy that the pin and assisted shoulder could rotate independently in different speed or even different direction during welding process. With the adjustment of rotation speed of pin and assisted shoulder, the heat production ratio between them could be rationally allocated, and the softening effects of thermal cycle would be effectively reduced. Hence, joints with excellent properties could be obtained.

✉ L. Zhou
zhouli@hitwh.edu.cn

[1] State Key Laboratory of Advanced Welding and Joining, Harbin Institute of Technology, Harbin 150001, China

[2] Shandong Provincial Key Laboratory of Special Welding Technology, Harbin Institute of Technology at Weihai, Weihai 264209, China

[3] Shanghai Aerospace Equipments Manufacturer Co. Ltd, Shanghai 200245, China

[4] State Key Laboratory of Advanced Metals and Materials, University of Science and Technology Beijing, Beijing 100083, China

At present time, limited studies have been done to investigate the microstructural evolution and mechanical properties of DR-FSWed joints. By fixing the assisted shoulder, stationary shoulder friction stir welding (SS-FSW) was proposed and researched by Widener et al. [18] and Crawford et al. [19]. Well-formed weld without visible flash and cavity defects was obtained under high rotation speed. Ji et al. [20] and Liu et al. [21] found the smaller shoulder affected zone of SS-FSW and attribute it to smaller diameter of rotational shoulder. Li et al. [22] performed SS-FSW on 5-mm-thick 6061-T6 aluminum alloy with different welding parameters and the optimal parameters are obtained at tool rotation speed of 1500 rpm and welding speed of 100 mm/min. The preliminary experiment of DR-FSW was conducted by Thomas et al. [17]. It was demonstrated that both peak temperature and high temperature residence time were reduced during welding process. Microstructure characteristics and mechanical properties of 2219-T6 aluminum alloy joint employing reverse dual-rotation friction stir welding (RDR-FSW) were reported by Li et al. [23–25]. The homogeneity of temperature field and microstructure were improved in RDR-FSW; therefore, joints with better properties can be obtained. Additionally, 3D model was developed by Shi et al. [26, 27] to study the process characteristics in RDR-FSW, including material flow field and thermal field.

Nevertheless, most of the studies focus on SS-FSW and RDR-FSW, with few papers reporting about co-rotating DR-FSW where the separated pin and shoulder rotate in one direction. Besides, the rotation speed of assisted shoulder, one important parameter that needs not to be considered in conventional FSW, plays a significant part in plastic material flow and heat generation in DR-FSW. Therefore, it is necessary to reveal the effects caused by the changing rotation speed of assisted shoulder on microstructure and mechanical properties of DR-FSWed joints. In the present study, 6061-T6 aluminum alloy was DR-FSWed with the pin and assisted shoulder rotating in one direction controlled by a self-developed tool system. The effects caused by the changing rotational speed on microstructural evolution and mechanical properties of the welded joints were investigated.

2 Experimental procedure

In this experiment, DR-FSW was conducted on 6061-T6 aluminum alloy plates with the dimension of 200 × 80 × 5 mm, whose chemical composition and mechanical properties are presented in Table 1. Welding was carried out on gantry type FSW machine developed in-house along the longitudinal direction of plates. Prior to welding, the mating edges were thoroughly milled and cleaned to avoid leaving any pollution in the joint.

Figure 1 illustrates the schematic view and assembly photo of the tool system for DR-FSW. Two primary sections were included in the system: pin and assisted shoulder. The taper threaded pin is connected with the spindle of FSW machine, while the assisted shoulder is driven by a servo motor and rotates independently. A gap of 0.1 mm is reserved between pin and assisted shoulder to avoid intense friction which might affect the stability of welding process. Meanwhile, a sub-size concave shoulder is designed on tool pin to impede the entry of plasticized materials into the gap. Previous studies demonstrated that well-formed joints with excellent properties could be obtained at the shoulder diameter of 14 mm in conventional FSW [24]; thus, the same shoulder diameter is applied as outer diameter of assisted shoulder in DR-FSW. The geometric dimensions of other main components are listed in Table 2.

In this experiment, the tool pin and assisted shoulder rotated in the same direction with different rotation speed. The shoulder plunge depth and tilt angle were maintained constant for all welded joints, which were respectively 0.1 mm and 3°. Meanwhile, the traverse speed and rotation speed of pin were respectively 200 mm/min and 1200 rpm, while the rotation speed of assisted shoulder varied from 0 to 1200 rpm in steps of 400 rpm. For simplicity, “AS” and “RS” are employed to represent the advancing side and retreating side of the joint, and rotation speed of pin and assisted shoulder are marked as “pin rotation speed” and “shoulder rotation speed” in subsequent sections. Particularly, when shoulder rotation speed reaches 1200 rpm which is equal to pin rotation speed, the function of DR-FSW is equal to that of conventional FSW.

The metallographic specimens were cut perpendicular to the welding direction by electrical discharge machining. They were examined by an OLYMPUS DSA 510 optical microscope after being etched with Keller reagent. The microhardness distribution was measured every 0.5 mm along the transverse weld centerline using a Vickers hardness tester. The testing load and loading time were constant at 100 g and 10 s during testing. The tensile specimen was prepared according to China National Standard GB/T 2649–2008 (Fig. 2). The tensile properties were estimated on an INSTRON 5967 mechanical tester at loading rate of 1 mm/min. To ensure the

Table 1 Chemical composition and mechanical properties of 6061-T6 aluminum alloy

Material	Chemical composition (wt.%)								Mechanical properties	
	Al	Mg	Si	Fe	Zn	Cu	Mn	Cr	Tensile strength (MPa)	Elongation (%)
6061-T6	Bal.	1.07	0.58	0.32	0.05	0.24	0.1	1.82	270	14

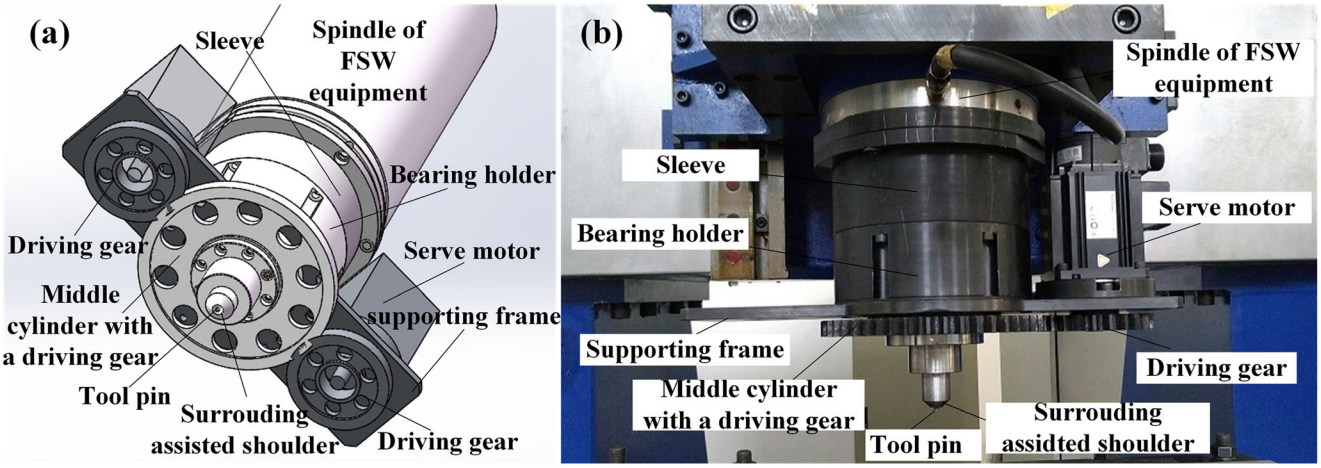

Fig. 1 Tool system for the DR-FSW. (**a**) Schematic view. (**b**) Setup photo

reliability of testing results, three samples for each parameter were employed. The characteristics of fracture surfaces were observed by TESCAN VEGAII scanning electron microscope.

3 Results and discussion

3.1 Heat production

During the welding process, heat input control is quite important to weld formation and resultant microstructure. In conventional FSW, the total heat generation by friction of contact surface can be expressed as below [28, 29]:

$$Q_{total} = \frac{2}{3}\pi\tau\omega_r\left(r_s^3 + 3r_p^2H_p\right) \quad (1)$$

where Q is the heat input, τ is the contact shear stress, ω_r is the tool rotation speed, r_s is the radius of shoulder, and r_p and H_p are the radius and length of pin. Furthermore, the heat generation could be divided into three parts (Fig. 3a), which are as follows [24]:

$$Q_1 = \frac{2}{3}\pi\tau\omega_r\left(r_s^3 - r_p^3\right) \quad (2)$$

$$Q_2 = 2\pi\tau\omega_r r_p^2 H_p \quad (3)$$

$$Q_3 = \frac{2}{3}\pi\tau\omega_r r_p^3 \quad (4)$$

Table 2 Dimensions of main components in the DR-FSW tool system

Sub-size concave shoulder		Tool pin		
Diameter (mm)	Concave angle (°)	Diameter at the end (mm)	Diameter at the root (mm)	Length (mm)
9.8	10	3.45	6.2	4.8

However, different from conventional FSW, the tool is divided into pin and assisted shoulder in DR-FSW. The heat generation is quite different which could be deduced from the above equation. The Q_1 could be split into Q_{1a} which is generated by assisted shoulder and Q_{1c} which is generated by sub-size concave shoulder in DR-FSW (Fig. 3b), while the Q_2 and Q_3 remain unchanged. The equation of Q_{1a}, Q_{1c}, and Q_{total}' are as follows:

$$Q_{1a} = \frac{2}{3}\pi\tau\omega_r\left(r_a^3 - r_c^3\right) \quad (5)$$

$$Q_{1c} = \frac{2}{3}\pi\tau\omega_a\left(r_c^3 - r_p^3\right) \quad (6)$$

$$Q_{total}' = \frac{2}{3}\pi\tau\left[\omega_r\left(r_c^3 + 3r_p^3H_p\right) + \omega_a\left(r_a^3 - r_c^3\right)\right] \quad (7)$$

In these equations, ω_a is shoulder rotation speed, and r_a and r_c are the radius of assisted shoulder and sub-size concave shoulder. It could be calculated that the ratio of heat generation at various

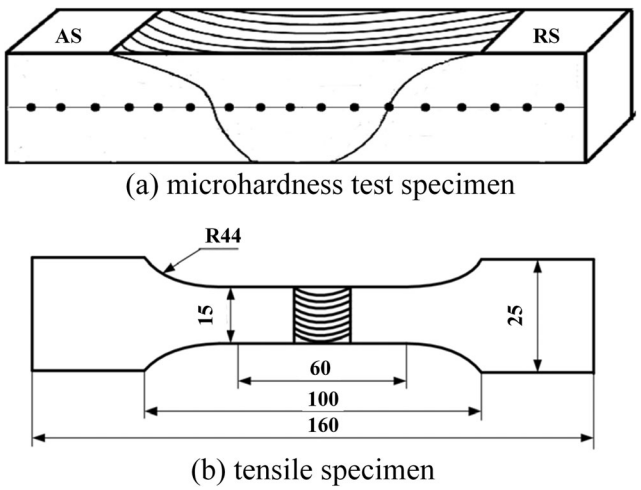

Fig. 2 Schematic illustration for dimension of transverse tensile specimen

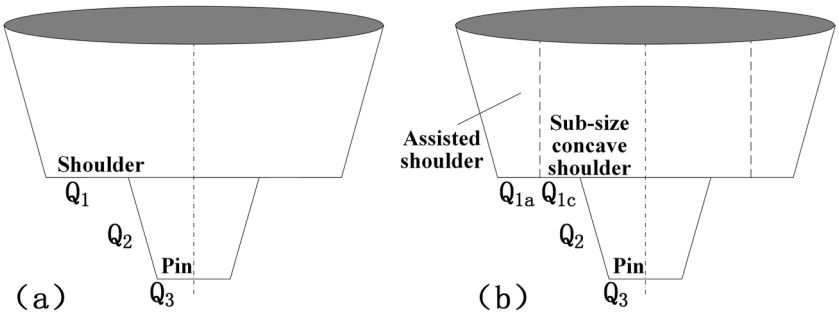

Fig. 3 Schematic of tool and interfaces of heat generation. (**a**) Conventional FSW. (**b**) DR-FSW

shoulder rotation speed from 0 to 1200 rpm is 1:1.43:1.87:2.30. It indicates that the heat input rapidly increases with shoulder rotation speed increasing, which would have a great impact on weld formation and resultant microstructure of joint.

3.2 Macroscopic characteristics

Figure 4 presents the surface appearances of joints at various shoulder rotation speed. Obviously, the joints obtained shows smooth surface without visible defects. There is little flash on the joints at the shoulder rotation speed of 0 and 400 rpm which indicates the effective hindering action of sub-size concave shoulder at low rotation speed. When the shoulder rotation speed continued to increase, the increasing heat input improved the thermoplastic material flow, and more plasticized aluminum was extruded out. As the consequence, superfluous flash on the joint is observed, especially at shoulder rotation speed of 1200 rpm.

The cross sections of the joint at various shoulder rotation speed are presented in Fig. 5. No typical defects such as voids and tunnels are found in the cross sections which indicate adequate heat input and sufficient material flow during welding process. Bowl-shaped weld zone with different width could be observed, and the width correspondingly broadens with the increase of shoulder rotation speed due to the increasing heat input. Although the faying surfaces were thoroughly milled and cleaned prior to welding, there are S-shaped curves observed in the joints probably owing to the oxidation of material in excessive temperature during welding process. According to previous studies, debates have long existed whether the S-shaped curve would impair the tensile properties of joint. Çam et al. [10] revealed that the S-shaped curve had no effect on the tensile properties of joint, although the fatigue performance was deteriorated. However, Chen et al. [30] proposed that the tensile properties were significantly affected by the S-shaped curve in which the tensile specimens fractured. In the present study, the S-shaped curve seems to have no effect on the tensile properties of welded joints which would be further discussed in the sections below.

3.3 Microstructure of welded joints

The joint welded by DR-FSW consists of four distinct zones: stirred zone (SZ), thermo-mechanically affected zone (TMAZ), heat-affected zone (HAZ), and base material (BM) just as the conventional FSWed joint [31]. To highlight the effect of shoulder, the SZ could be further divided into weld nugget zone (WNZ) and shoulder affected zone (SAZ). Influenced thermally and mechanically to various degrees, microstructural evolution in various zones are quite different causing grains with different morphology and size after welding (Fig. 6). The BM (Fig. 6b) consists of coarse and elongated grains with Si-rich precipitation phases evenly distributed [14]. The HAZ (Fig. 6c) was only exposed to the thermal cycle, and the grains were free from plastic deformation and dynamic recrystallization during welding. Hence, the HAZ retains almost the same microstructure as that in BM, while slight grain coarsening occurred with coarsening and dissolution of precipitation phases. As to the

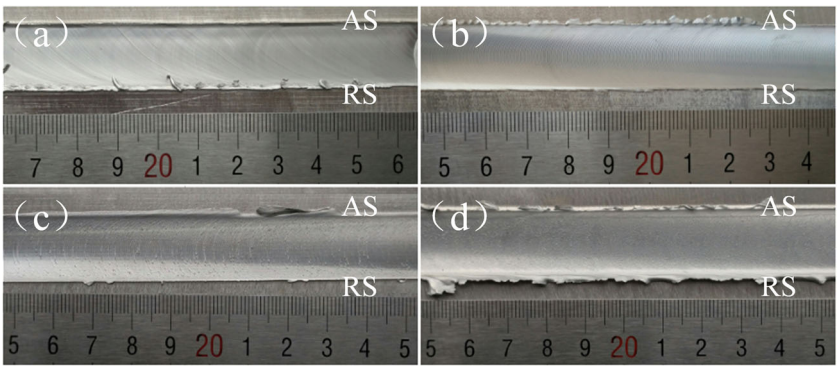

Fig. 4 Surface appearance of the joints at shoulder rotation speed of (**a**) 0 rpm, (**b**) 400 rpm, (**c**) 800 rpm, and (**d**) 1200 rpm

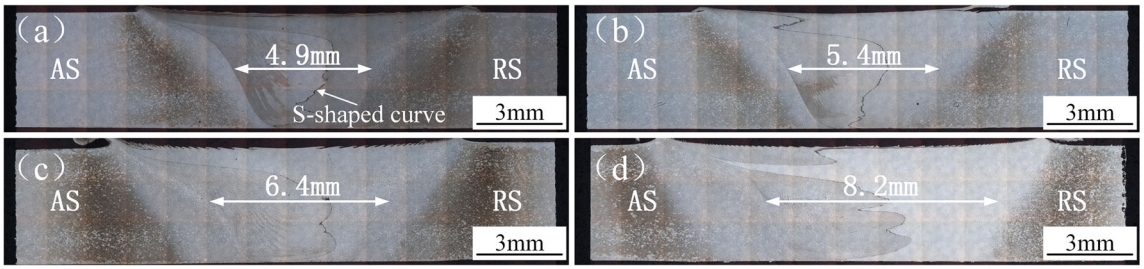

Fig. 5 Cross sections of the joints at shoulder rotation speed of (**a**) 0 rpm, (**b**) 400 rpm, (**c**) 800 rpm, and (**d**) 1200 rpm

TMAZ, deformation and partial dynamic recrystallization happened (Fig. 6d) due to insufficient deformation rate and thermal effect, which caused refined and elongated grains in this region. Additionally, precipitation phases were partially dissolved and split because of the thermo-mechanical action in the TMAZ [14]. The WNZ (Fig. 6e) and SAZ (Fig. 6f) experienced high thermal cycle and intense plastic flow during welding; thus, significant dynamic recrystallization occurred which leads to the formation of fine-grained microstructure. The precipitation phases in the WNZ and SAZ are generally larger than those in the BM, which implies the occurrence of coarsening and dissolution of precipitation phases at the high temperature environment during FSW process [31]. Meanwhile, the grain sizes of WNZ and SAZ are quite different on account of various heat input and deformation rate, and the details will be discussed in the following part. The high magnification of S-shaped curve mentioned above is given in Fig. 6g.

Figure 7 shows the microstructure of HAZ and TMAZ at various shoulder rotation speeds. There is no obvious difference in the HAZ obtained at various shoulder rotation speed, which indicates that the change of heat input has little influence on grain size in HAZ. In regard to TMAZ, the higher heat input results in coarser grains as shoulder rotation speed increases. Moreover, the increase of heat input promotes the plastic material flow which increases the grain deformation degree in the TMAZ. As a result, the transition interface between WNZ and TMAZ gradually weakens.

The microstructures of SAZ and WNZ under various shoulder rotation speed are presented in Figs. 8 and 9. Fine recrystallized equiaxed grains are obtained with different average grain

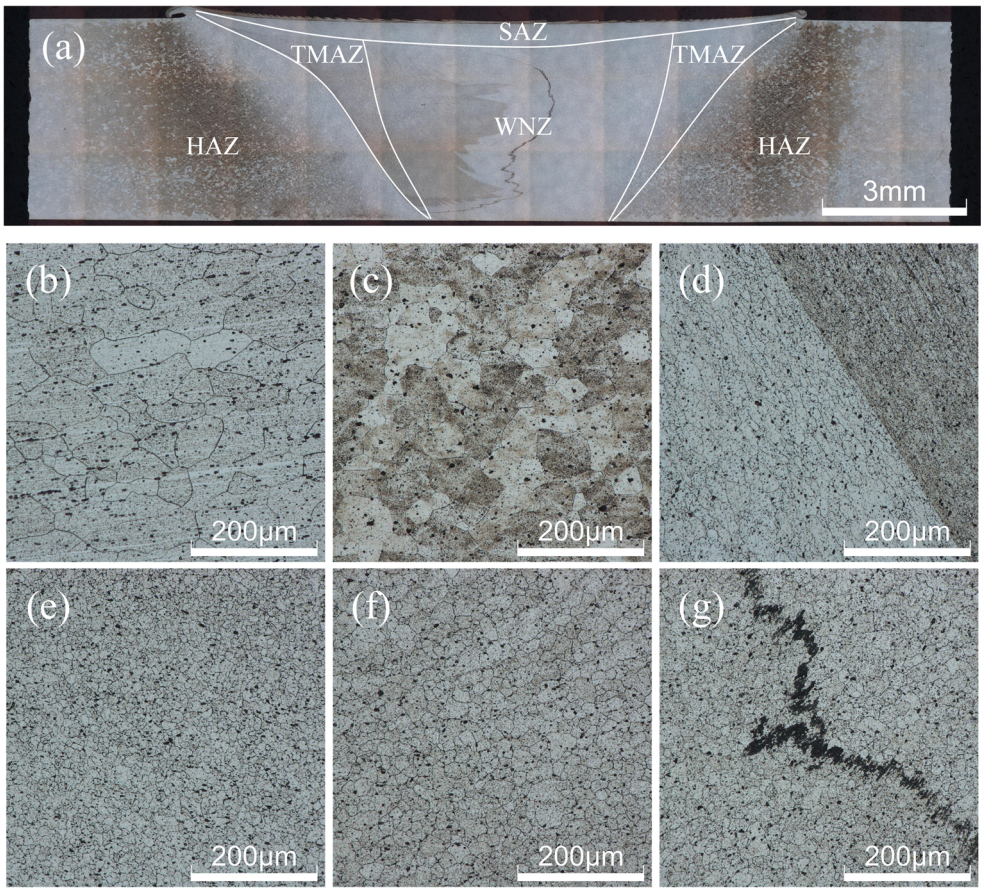

Fig. 6 Typical optical micrographs of different regions of DR-FSWed joint. (**a**) Macroscopic appearance. (**b**) BM. (**c**) HAZ. (**d**) TMAZ. (**e**) SAZ. (**f**) WNZ. (**g**) S-shaped curve

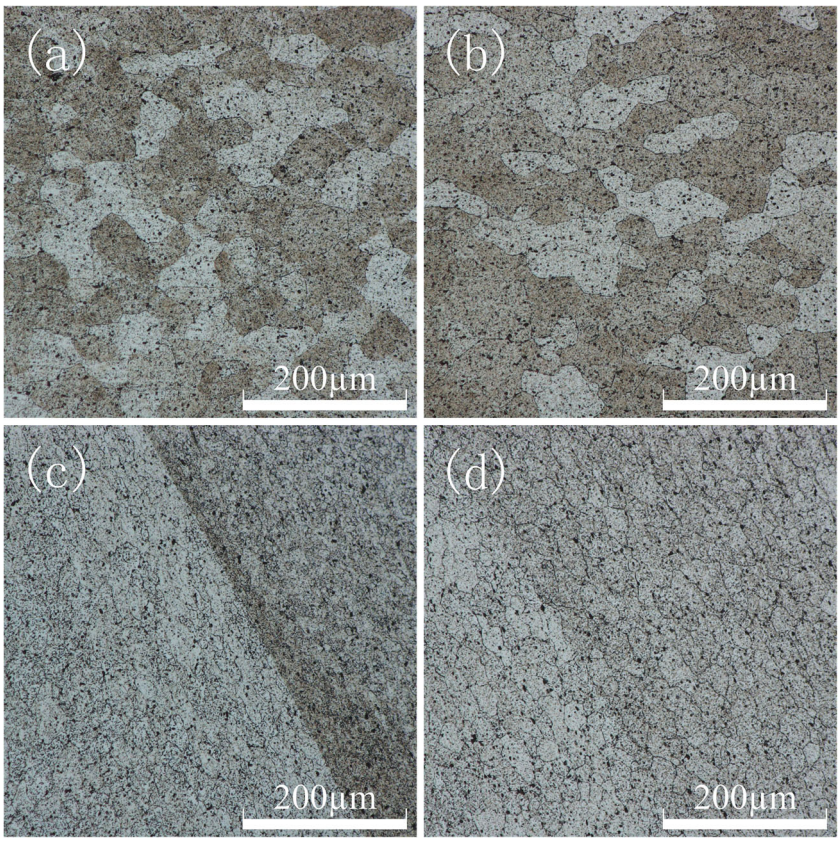

Fig. 7 Microstructure of joint in the section of (**a**) HAZ in the 0 rpm joint, (**b**) HAZ in the 1200 rpm joint, (**c**) TMAZ in the 0 rpm joint, and (**d**) TMAZ in the 1200 rpm joint

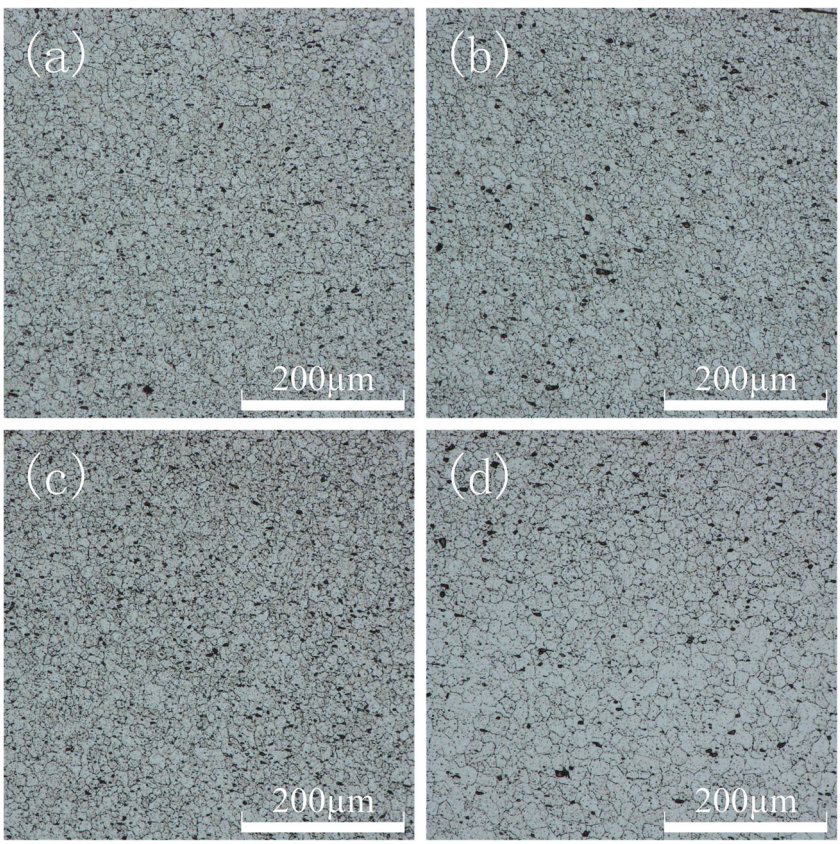

Fig. 8 Microstructure of SAZ at shoulder rotation speed of (**a**) 0 rpm, (**b**) 400 rpm, (**c**) 800 rpm, and (**d**) 1200 rpm

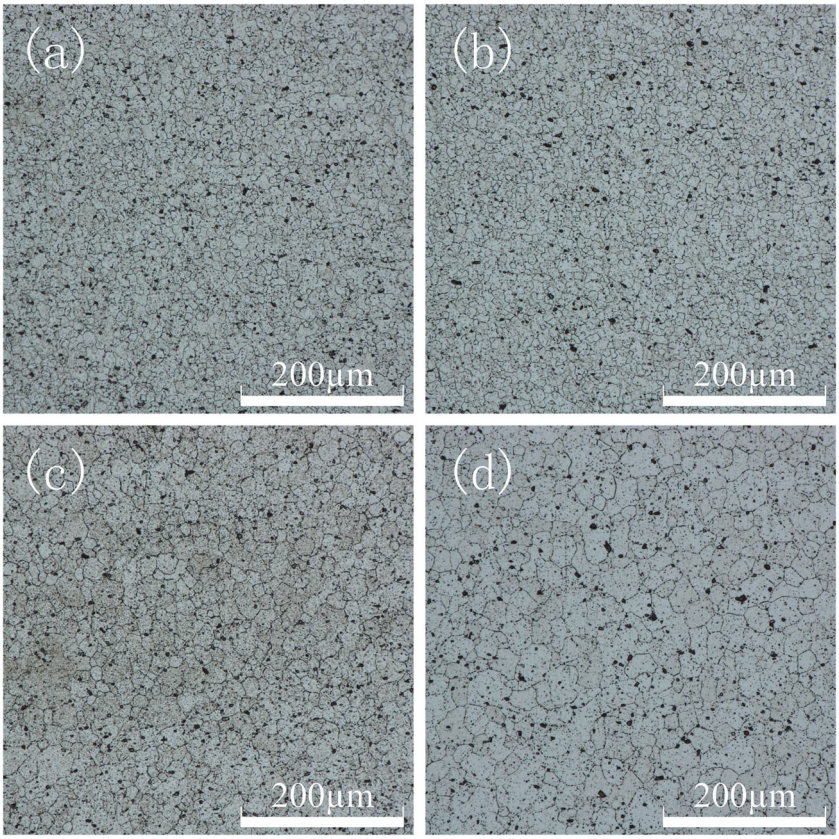

Fig. 9 Microstructure of WNZ at shoulder rotation speed of (**a**) 0 rpm, (**b**) 400 rpm, (**c**) 800 rpm, and (**d**) 1200 rpm

size in both two zones. When shoulder rotation speed increases from 0 to 1200 rpm, the average size of refined grains in SAZ is measured to be 11.97, 12.66, 14.32, and 16.53 μm, respectively, while it is 12.71, 13.08, 20.3, and 24.00 μm in WNZ (Fig. 10). The grain size increases with increasing shoulder rotation speed in both two zones due to the increasing heat input, although there is little change when rotation speed increases from 0 to 400 rpm. It is observed that the grain size in WNZ is larger than that in SAZ at same shoulder rotation speed, which is completely opposite to the phenomenon observed by Li et al. [24]. The welding parameters and rotation direction of assisted shoulder employed in this experiment are quite different to theirs which caused different heat input and deformation rate. Thus, the grain size of resultant microstructure is quite different which could be explained by Zener-Hollomon parameter.

According to the Zener-Hollomon parameter, the grain size of resultant microstructure is dependent on both heat input and

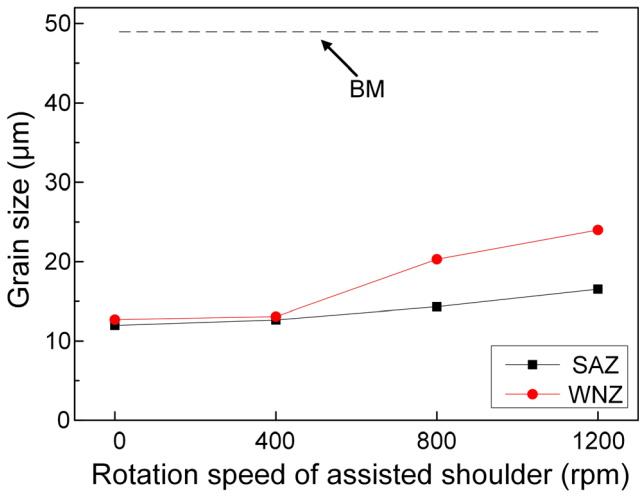

Fig. 10 Effect of shoulder rotation speed on grain size in SAZ and WNZ

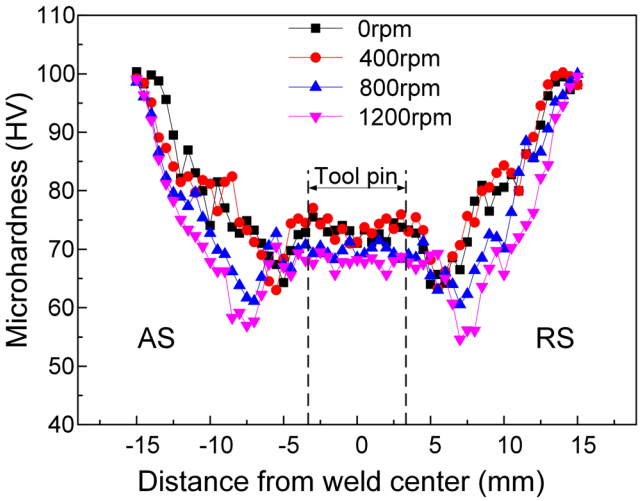

Fig. 11 Microhardness distribution on the transverse cross section of the typical joint at various shoulder rotation speed

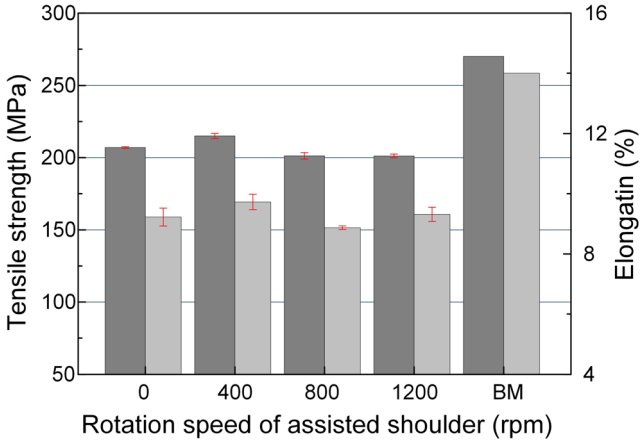

Fig. 12 Transverse tensile strength of joints at different shoulder rotation speed

deformation rate [32]. On the one hand, higher heat input generated at high shoulder rotation speed promotes the grain growth which increases the grain size. On the other hand, increasing shoulder rotation speed brings about great deformation rate which promotes the dynamic recrystallization. That is, there is a competitive relationship between the two factors to impact the resultant grain size. It is clear that the SAZ is subject to the pin and assisted shoulder in this experiment, while WNZ is only affected by pin. Although the heat input in SAZ is large enough to promote the grain growth, higher deformation rate obtained would promote dynamic recrystallization to acquire much finer grains. Therefore, the resultant grain in SAZ is smaller than that in WNZ. It indicates that the deformation rate plays a dominant role in resultant grain size rather than heat input.

3.4 Microhardness distribution across the joints

The microhardness of heat-treatable aluminum alloy is mainly dependent on precipitation phase distribution and grain size [19]. Figure 11 shows the microhardness distribution across the joints at various shoulder rotation speed. A softened zone including SAZ, WNZ, TMAZ, and HAZ formed after welding owing to the coarsening and dissolution of precipitation phases with strengthening effect on the matrix [31]. The microhardness profile displays a "W" type with the maximum value reached in the BM and the minimum value found in the HAZ [16, 19]. This could be attributed to different microstructural evolutions in various zones during DR-FSW process. In the softened zone, finer equiaxed recrystallized grains are observed in the WNZ; accordingly, the hardness is much larger than other regions in accordance with Hall-Petch equation. The grain in TMAZ is a little larger than that in WNZ, for which the hardness is lower than that in WNZ. The HAZ is affected by welding thermal effect; consequently, coarsened grains are obtained in this zone which causes the hardness value to decrease.

The joints at various shoulder rotation speed show the same profile, "W" shape, while the microhardness value varies a lot. As the shoulder rotation speed increases, the microhardness of weld zone gradually decreases which is attributed to the increasing grain size. Furthermore, the lowest hardness lies in the area which is about 5 mm distant from weld center at shoulder rotation speed of 0 rpm, while it is measured to be 7.5 mm when shoulder rotation speed increases to 1200 rpm. That is to say, with the increase of shoulder rotation speed, the width of soften region becomes larger. This difference could be explained by the increasing role of assisted shoulder on heat input.

3.5 Transverse tensile strength of the joint

The transverse tensile properties of joints under various shoulder rotation speed are illustrated in Fig. 12. The tensile strength and elongation are measured to be 202 MPa (74.7% of the BM) and 9.31% (66.5% of the BM) in this experiment using conventional FSW, where the shoulder rotation speed is 1200 rpm. When the DR-FSW is applied, the tensile strength and elongation increase and reach the maximum values at shoulder rotation speed of 400 rpm, which are 219 MPa (81.1% of the BM) and 9.97% (71.2% of the BM). Remarkably, the lowest tensile strength obtained is 201 MPa (74.4% of the BM) at shoulder rotation speed of 800 rpm, which is roughly equal to that of conventional FSW. Conclusion could be reached that well-behaved FSW joint could be acquired using DR-FSW, and tensile properties of welded joint at optimum parameter could be significantly improved.

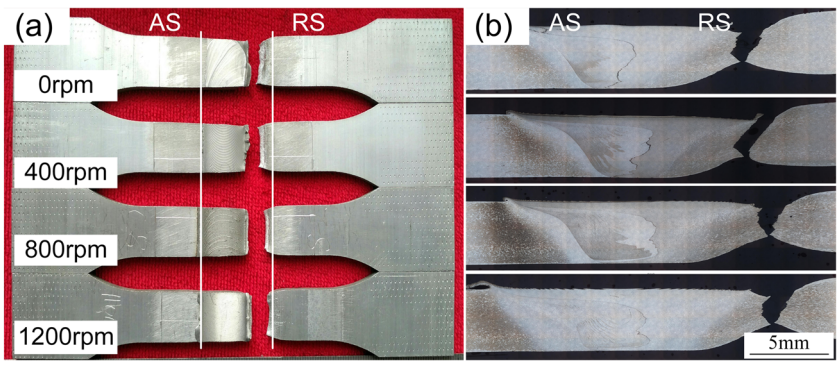

Fig. 13 Fracture location of the joints at various shoulder rotation speed. (**a**) Failed tensile specimens. (**b**) Cross sections

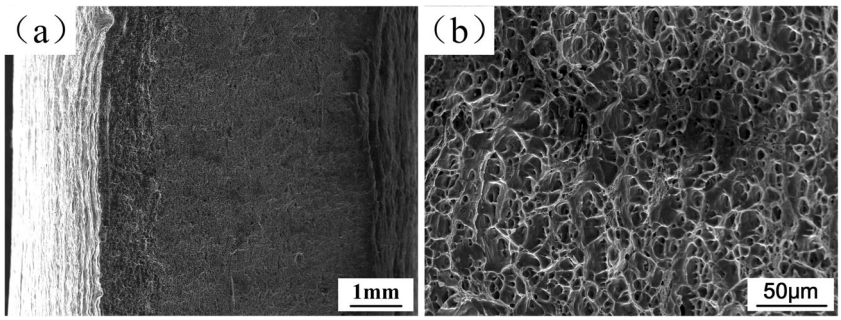

Fig. 14 Tensile fracture morphologies of the fractured specimen at shoulder rotation speed of 400 rpm. (**a**) Overall morphology. (**b**) High magnification

All tensile specimens failed at the interface of HAZ and TMAZ on the RS (Fig. 13). It is largely correspond with the coarsened grains in HAZ for the influence of welding thermal cycle. Meanwhile, thermoplastic material moved from AS to RS and transferred parts of heat during the welding process, which leads to higher temperature on the RS. The coarser grains on the RS were obtained which resulted in lowest microhardness in this region in which the fracture occurred [15]. Figure 14 presents the typical tensile fracture morphologies of the fractured specimen at optimum parameter. A uniform fracture section of joint is observed, and fine dimples and tearing edges are found in high magnification which manifests that the facture mechanism is micropore aggregation fracture.

4 Conclusion

In the present study, 6061-T6 aluminum alloy was DR-FSWed using self-designed tool system at constant traverse speed of 200 mm/min and pin rotation speed of 1200 rpm with shoulder rotation speed ranging from 0 to 1200 rpm. The effects of shoulder rotation speed on microstructural evolution and mechanical properties of joints were investigated. Defect-free joints were gained as the size of weld zone enlarged with increasing shoulder rotation speed. SAZ and WNZ were characterized by fine recrystallized grains, and the grain size gradually increased with shoulder rotation speed, while the grain size in SAZ was much smaller. The microhardness distribution profile was greatly affected by shoulder rotation speed with the highest value located at BM and lowest value located at HAZ, and the hardness increased with the increase of shoulder rotation speed. The maximum tensile strength and elongation obtained at shoulder rotation speed of 400 rpm were 215 MPa and 9.72%, which are higher than that obtained by conventional FSW. All welded joints fractured at the interface of HAZ and TMAZ which is characterized by ductile fracture.

Funding information The research was sponsored by the National Natural Science Foundation of China (No. 51775143), the National Science and Technology Major Project (No. 2017ZX04005001), the National Defense Industrial Technology Development Program (No. JCKY2017203B066), and the State Key Lab of Advanced Metals and Materials (No. 2017-Z06).

References

1. Miller WS, Zhuang L, Bottema J, Wittebrooda AJ, Smetb PD, Haszlerc A, Viereggec A (2000) Recent development in aluminium alloys for the automotive industry. Mater Sci Eng A 280(1):37–49
2. Dursun T, Soutis C (2014) Recent developments in advanced aircraft aluminium alloys. Mater Des 56(4):862–871
3. Lakshminarayanan AK, Balasubramanian V, Elangovan K (2009) Effect of welding processes on tensile properties of AA6061 aluminium alloy joints. Int J Adv Manuf Technol 40(3–4):286–296
4. Sánchez-Amaya JM, Delgado T, González-Rovira L, Botana FJ (2009) Laser welding of aluminium alloys 5083 and 6082 under conduction regime. Appl Surf Sci 255(23):9512–9521
5. Ion JC (2013) Laser beam welding of wrought aluminium alloys. Sci Technol Weld Join 5(5):265–276
6. Rohde M, Markert C, Pfleging W (2010) Laser micro-welding of aluminum alloys: experimental studies and numerical modeling. Int J Adv Manuf Technol 50(1–4):207–215
7. Sheikhi M, Ghaini FM, Assadi H (2015) Prediction of solidification cracking in pulsed laser welding of 2024 aluminum alloy. Acta Mater 82:491–502
8. Thomas WM (1991) Friction stir butt welding. International Patent Application No. PCT/GB92/0220
9. Threadgill PL, Leonard AJ, Shercliff HR, Withers PJ (2009) Friction stir welding of aluminium alloys. Int Mater Rev 54(2):49–93
10. Çam G, Mistikoglu S (2014) Recent developments in friction stir welding of Al-alloys. J Mater Eng Perform 23(6):1936–1953
11. Çam G, İpekoğlu G (2016) Recent developments in joining of aluminum alloys. Int J Adv Manuf Technol 91(5–8):1–16
12. Ma ZY, Feng AH, Chen DL, Shen J (2017) Recent advances in friction stir welding/processing of aluminum alloys: microstructural evolution and mechanical properties. Crit Rev Solid State 43(1):1–65
13. Shah PH, Badheka VJ (2017) Friction stir welding of aluminium alloys: an overview of experimental findings—process, variables, development and applications. P I Mech Eng L-J Mat
14. Murr LE, Liu G, Mcclure JC (1998) A TEM study of precipitation and related microstructures in friction-stir-welded 6061 aluminium. J Mater Sci 33(5):1243–1251
15. Liu H, Maeda M, Fujii H, Nogi K (2003) Tensile properties and fracture locations of friction-stir welded joints of 1050-H24 aluminum alloy. J Mater Sci Lett 22(1):41–43
16. Rajakumar S, Muralidharan C, Balasubramanian V (2011) Predicting tensile strength, hardness and corrosion rate of friction stir welded AA6061-T6 aluminium alloy joints. Mater Des 32(5): 2878–2890

17. Thomas WM, Norris IM, Staines DG, Watts ER (2012) Friction stir welding—process developments and variant techniques. Weld Int 17(11):852–855
18. Widener CA, Talia JE, Tweedy BM, Burford DA (2006) High-rotational speed friction stir welding with a fixed shoulder. Proceedings of 6th International Friction Stir Welding Symposium; Montreal, Canada
19. Crawford R, Bloodworth T, Cook GE, Strauss AM, Hartman DA (2006) High speed friction stir welding process modeling. In: 6th International Symposium on Friction Stir Welding, Montreal, Canada, 10–13 October
20. Ji SD, Meng XC, Liu JG, Zhang LG, Gao SS (2014) Formation and mechanical properties of stationary shoulder friction stir welded 6005A-T6 aluminum alloy. Mater Des 62(10):113–117
21. Liu HJ, Li JQ, Duan WJ (2013) Friction stir welding characteristics of 2219-T6 aluminum alloy assisted by external non-rotational shoulder. Int J Adv Manuf Technol 64(9–12):1685–1694
22. Li D, Yang X, Cui L, He F, Shen H (2014) Effect of welding parameters on microstructure and mechanical properties of AA6061-T6 butt welded joints by stationary shoulder friction stir welding. Mater Des 64:251–260
23. Li JQ, Liu HJ (2013) Characteristics of the reverse dual-rotation friction stir welding conducted on 2219-T6 aluminum alloy. Mater Des 45(6):148–154
24. Li JQ, Liu HJ (2013) Effects of welding speed on microstructures and mechanical properties of AA2219-T6 welded by the reverse dual-rotation friction stir welding. Int J Adv Manuf Technol 68(9–12):2071–2083
25. Li JQ, Liu HJ (2015) Effects of the reversely rotating assisted shoulder on microstructures during the reverse dual-rotation friction stir welding. J Mater Sci Technol 31(4):375–383
26. Shi L, Wu CS, Liu HJ (2014) Numerical analysis of heat generation and temperature field in reverse dual-rotation friction stir welding. Int J Adv Manuf Technol 74(1–4):319–334
27. Shi L, Wu CS, Liu HJ (2014) Modeling the material flow and heat transfer in reverse dual-rotation friction stir welding. J Mater Eng Perform 23(8):2918–2929
28. Schmidt H, Hattel J, Wert J (2014) An analytical model for the heat generation in friction stir welding. Model Simul Mater Sci Eng 12(1):143
29. Khandkar MZH, Khan JA, Reynolds AP (2003) Prediction of temperature distribution and thermal history during friction stir welding: input torque based model. Sci Technol Weld Join 8(3): 165–174
30. Chen HB, Yan K, Lin T, Chen SB, Jiang CY, Zhao Y (2006) The investigation of typical welding defects for 5456 aluminum alloy friction stir welds. Mater Sci Eng A 433(1–2):64–69
31. Chen YC, Liu HJ, Feng JC (2006) Friction stir welding characteristics of different heat-treated-state 2219 aluminum alloy plates. Mater Sci Eng A 420(1–2):21–25
32. Hu HE, Zhen L, Yang L, Shao WZ, Zhang BY (2008) Deformation behavior and microstructure evolution of 7050 aluminum alloy during high temperature deformation. Mater Sci Eng A 488(1–2):64–71